

Baseline Issues in an Airborne 650 GHz Radiometer

A. Murk, N. Kämpfer

Institute of Applied Physics, University of Bern

Abstract

We describe the effects of baseline ripple in an airborne submillimeter wave radiometer, which are caused by standing waves in the quasi-optical path. These baselines can be reduced with an improvement of the calibration loads and with a pathlength modulator. We have modelled the impact of the baseline on the retrieval of the volume mixing ratio profiles of the atmospheric constituents and we will discuss a method for the baseline removal during the inversion process.

Keywords: submillimeter wave radiometry, baseline ripple, calibration loads

1 Introduction

Remote sensing with millimeter and submillimeter wave radiometers is an important tool in atmospheric research. Since the errors from the radiometric noise of the receiver can be reduced with low noise receivers and long integration times, the measurements are often limited by the systematic baseline errors. These are all deviations of the measured power spectra from the true atmospheric signal, which can be caused by different instrumental effects. Among these are the nonlinearities in any of the components of the receiver and the differential nonlinearities of the spectrometer. These errors can be reduced by using a balanced calibration scheme instead of a total power calibration of the radiometer [14]. Another possible error source is the response of the mixer to harmonic sidebands [10]. In this paper we will focus only on the baseline caused by standing waves in the quasi-optics.

Most receivers are calibrated with a periodical beam switching between the signal and two reference loads at different physical temperatures. Following the conventions of microwave radiometry [16] the spectral power densities are usually expressed as equivalent brightness temperature T . In the case of a total power calibration the unknown brightness temperature of the sky T_A is calculated from the measurement of the atmospheric signal P_A and the measurements P_C and P_H of the cold and the hot reference loads:

$$T_A = \frac{P_A - P_C}{P_H - P_C} (T_H - T_C) + T_C \quad (1)$$

Typical calibration loads are microwave Absorbers at ambient temperature and immersed in liquid nitrogen, which are assumed to behave like a perfect black body. Reflections from these absorbers induce a Fabry-Pérot type resonance which results in a frequency dependent modulation in the detected power. Phase and period of this ripple is given by the distance d within the resonant structure, while the amplitude is determined by the reflection coefficients Γ and the brightness temperatures of the receiver and the load, respectively. When the reflectivities are small, the modulated component of the detected noise power can be approximated by [8]:

$$\Delta T = 2 (T_{Receiver} - T_{Load}) \Gamma_{Load} \Gamma_{Receiver} \cos \left(4\pi\nu \frac{d}{c} + \Phi \right) \quad (2)$$

where: ν = frequency
 c = velocity of light
 Φ = arbitrary phase term
 Γ = reflection coefficients for the electric field at the receiver and the load
 d = distance between receiver and load
 T_{Load} = brightness temperature of the load
 $T_{Receiver}$ = brightness temperature radiated out of the receiver

According to equation 1 the standing waves from each of the three measurements will contribute to the total baseline, depending on the three brightness temperatures. In a balanced radiometer, which uses a reference measurement P_{Ref} with $T_{Ref} \approx T_A$ for the calibration, the standing waves from the hot and the cold calibration load can be neglected. Also all baseline components which are identical in the signal and the reference measurements are removed. But since the optical path has to be changed between the two measurements, a certain amount of baseline ripple will remain in most cases.

2 Instrumental Description

A schematic diagram of the airborne 650 GHz receiver is shown in figure 1. It was developed for the detection of stratospheric ClO, HCl and O₃ within the Submm Limb Sounder Technology Program of the European Space Agency ESA/ESTEC. The frontend consists of a cooled Schottky diode mixer and a 637.2 GHz local oscillator, both fabricated by the *Radiometer Physics GmbH*. In the quasi-optical path two Martin-Puplett interferometers are used as a diplexer and as a tunable single sideband filter. They were developed at the University of Bremen at an earlier stage of the ESA project [1]. The reference loads are made of two microwave absorbers *Eccosorb-CV 3* from (Emerson&Cuming), one in liquid nitrogen and one in a heated enclosure. A rotating calibration mirror is used to switch between these loads and the atmospheric signal from the aircraft window. The frontend also includes a pathlength modulator to reduce the effects from the standing waves. This unit will be described in section 3.

The submillimeter wave radiation is down-converted to an intermediate frequency (IF) band between 10.5-14.5 GHz and amplified with a cooled HEMT amplifier. After further amplification, mixing and filtering in the IF conditioner the signals are analysed by an acousto-optical spectrometer (AOS, from *Meudon Observatory*) with 1 GHz bandwidth and 1 MHz resolution and by a chirp-transform spectrometer (CTS, from *DASA and MPAE*) with 180 MHz bandwidth and 280 kHz resolution. The noise temperature of the receiver is about 3000 K in single sideband operation. Further details about the system and the results from the flight campaigns are given in [11].

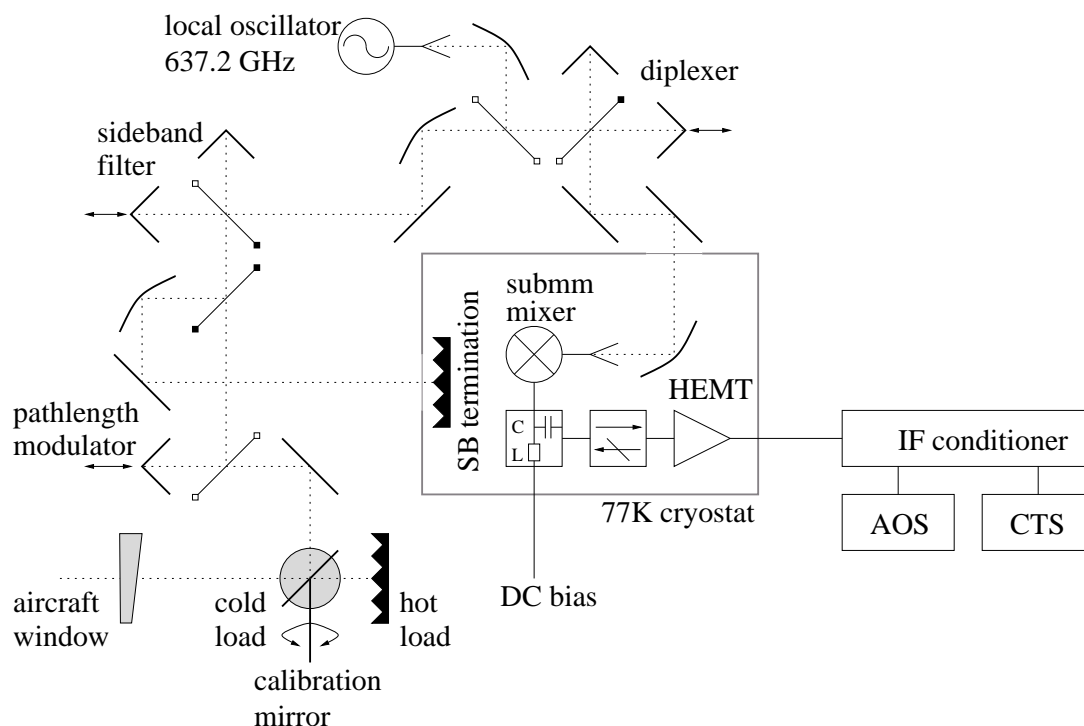


Figure 1: Schematic setup of the 650 GHz receiver

3 Pathlength Modulator

A commonly used technique for the baseline reduction is a periodical phase shift of the standing waves during the integration time. This can be achieved by inserting a rotating dielectric disk in the signal path [4], or by modulating the distance d with a moving mirror [6]. In many radiometers a reciprocating mirror with an eccentric drive is used for that purpose, which results in an sinusoidal change of the form $\Delta d(t) = d_0 \sin(\omega t)$.

The pathlength modulator in our setup consists of a polarising wire grid and a rooftop mirror, whose symmetrical axis is aligned under an angle of 45° with respect to the wires. The mirror is mounted on a translation stage which can be moved with a piezo-electrical actuator over a distance up to $300 \mu\text{m}$. An integrated strain-gauge sensor allows a precise measurement of the actual mirror position. The motion of the mirror is defined with a function generator, which can apply an alternating voltage of either a sinusoidal or a rectangular waveform on the piezo crystal.

The standing waves in the integrated spectra are cancelled only at certain modulation amplitudes. The factor γ of the baseline reduction for a given wavelength λ can be calculated from the time average of equation 2:

$$\gamma = \frac{\omega}{2\pi} \int_0^{2\pi/\omega} \cos\left(4\pi \frac{d + \Delta d(t)}{\lambda}\right) dt \quad (3)$$

For the sinusoidal waveform the solution of this integral is given by [6]:

$$\gamma = J_0\left(4\pi \frac{d_0}{\lambda}\right), \quad (4)$$

where J_0 is the zero order Bessel function. To achieve an optimum baseline reduction the modulation amplitude has to be set to an value where $4\pi d_0/\lambda$ corresponds to a zero crossing of the Bessel function. In the case of the rectangular waveform Δd is changed linear in time between 0 and d_0 , which results in:

$$\gamma = \frac{\sin\left(4\pi \frac{d_0}{\lambda}\right)}{4\pi \frac{d_0}{\lambda}} \quad (5)$$

Here the baseline vanishes if d_0 is an integer multiple of $\lambda/4$. Figure 2 shows the baseline reduction of both waveforms for different values of d_0 .

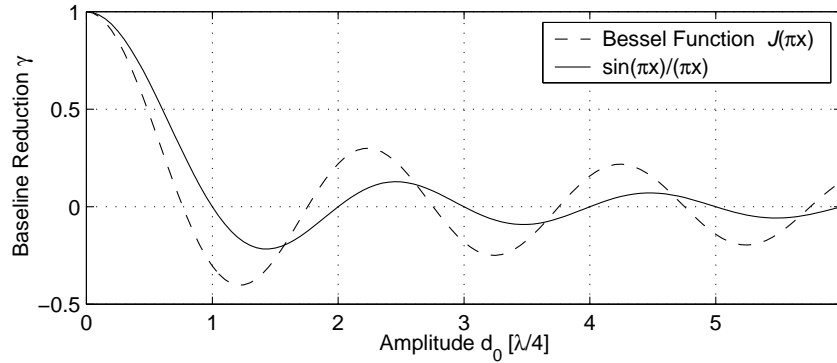


Figure 2: Baseline reduction for the different operational modes of the pathlength modulator. In this figure the modulation amplitude d_0 is expressed in units of $\lambda/4$.

Since the modulation amplitude has to be optimised for a certain wavelength, it is not possible to achieve a full baseline reduction over the whole bandwidth. It can be shown that the frequency dependence of γ is independent of the choice of the zero crossing for the linear motion, while it is getting worse at larger modulation amplitudes for the sinusoidal case. But γ is still smaller than 0.1 % over a bandwidth of 1 GHz for the first zero crossing of both functions.

A much stronger degradation of the baseline reduction is caused by a small deviation of d_0 from the ideal value. Again it can be shown that the linear motion is less sensitive to these errors, but now the performance of the pathlength modulator can be improved with the choice of a higher order of the zero crossings in both cases.

The pathlength modulator of the airborne 650 GHz radiometer was tested with a measurement of a flat aluminum sheet at the input of the receiver. It produces a strong baseline of about 100 K amplitude. As indicated in figure 3, in this case the baseline amplitude could be reduced by a factor of 20 using the linear motion.

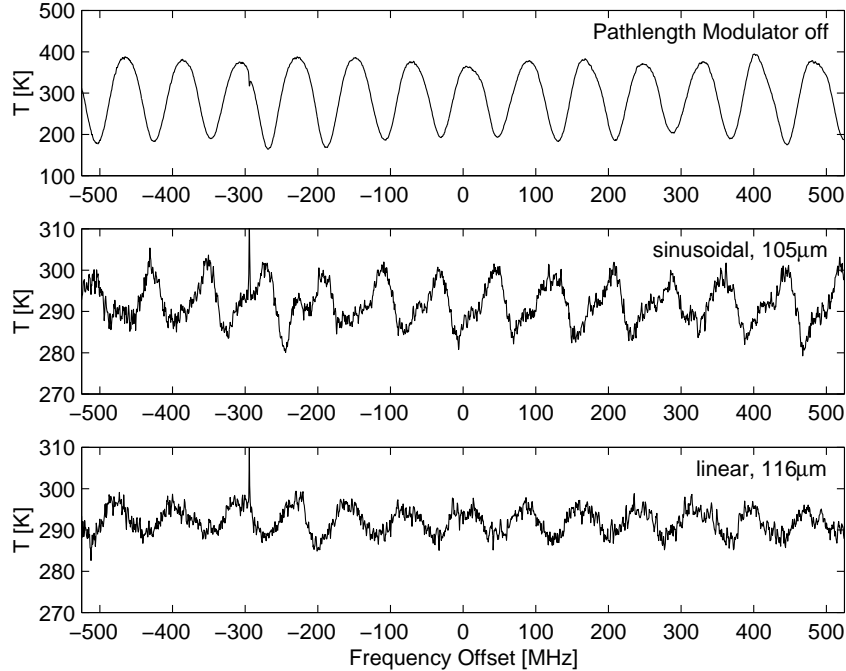


Figure 3: Measurement of a flat aluminum plate without the pathlength modulator and with a sinusoidal and a linear motion of the reciprocating mirror.

4 Calibration Loads

The amplitude of the standing waves is related closely to the reflectivity of the microwave absorbers in the calibration loads. Commercially available materials include carbon loaded polyurethane foams [2], carbon loaded polypropylene [17], silicon based absorbers [3] and rigid absorbers with a ferrite loading [2]. Most of them have a shaped surface to achieve a low reflectivity.

To demonstrate the varying performance of these materials figure 4 displays the observed baselines produced by different absorbers. The TK-RAM from *Thomas Keating Ltd.* has a pyramidal shaped surface tailored especially for submillimeter waves, while the flat foam absorber AN-72 from *Emerson&Cuming* is less suited for these applications. A comparison of the standing waves from other materials can be found in [12].

The drawback of the foam and polypropylene based absorbers for spaceborn and cryogenic applications is their low thermal conductivity and their outgassing problems. These problems can be overcome with castable rigid absorbers like CR-110 from *Emerson&Cuming*. But these materials have a bad matching to free space and therefore have to be shaped very carefully.

Within the ESA Submm Limb Sounder Technology Program the companies *AEA Technology* and *Thomas Keating Ltd.* have developed such a calibrated hot load (CHL) for the 0.4 - 1 THz range. Details on the conical design of the load are given in [7]. Several methods were proposed to test the performance of this load, but the stringent requirements on their reflectivity have proved to be difficult to verify.

We have used a quasi-optical reflectometer together with a submillimeter network analyser from *AB-Millimetre* for that purpose. The reflectometer as shown in figure 5 consists of a quasi-optical 3 dB coupler, realized with

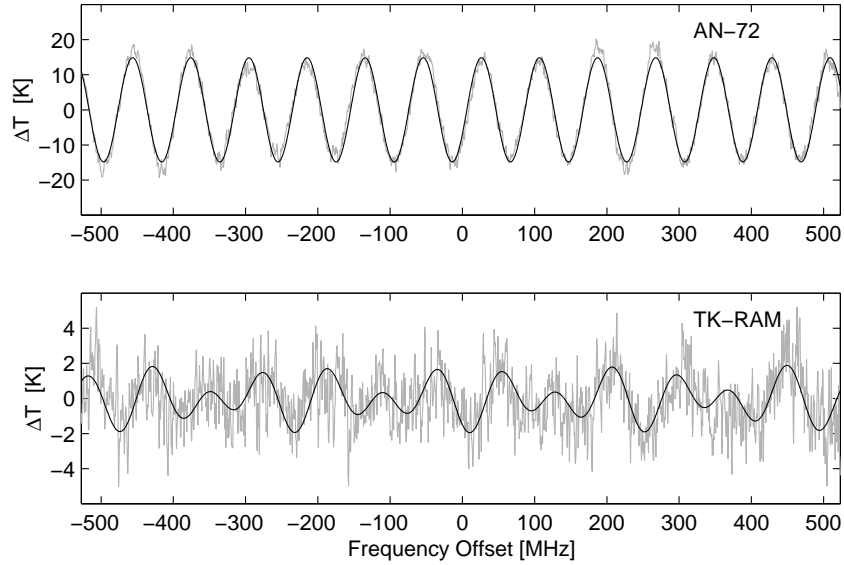


Figure 4: Baselines from different microwave absorbers at normal incidence and a centre frequency of 648 GHz

two polarising wire grids. Corrugated horns and elliptical mirrors form a well defined gaussian beam with an beam waist $\omega_0 = 10$ mm close to the target under investigation. The ABmm network analyser allows a true vector measurement up to 1 THz using a phase-locked and multiplied gunn oscillator as a source and a harmonic detection scheme with a similar phase-locked local oscillator [5].

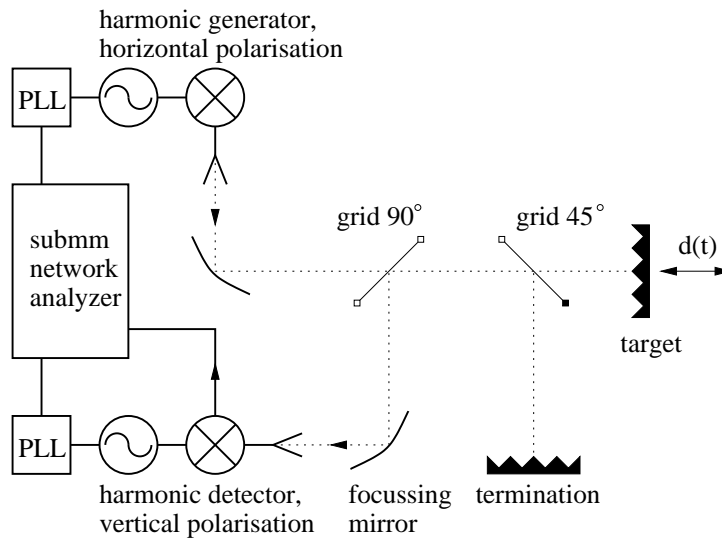


Figure 5: Measurement setup for the determination of the monostatic reflectivity of an absorber target.

With this setup the detected signal is a superposition of the reflections from the target and the absorber at the termination. To separate the two components a phase change is introduced by a slow movement $d(t)$ of the target. This results in the periodic structure of the CHL measurement in figure 6, where the loads were moved for about 5 wavelengths during the 60 s of the observation. In polar coordinates and on a linear scale the data points of each target are laying on a circle, which has a radius corresponding to the reflection coefficient Γ of the load. This is shown in figure 7 for the CHL measurement, from which a very low reflectivity of -69 dB can be deduced.

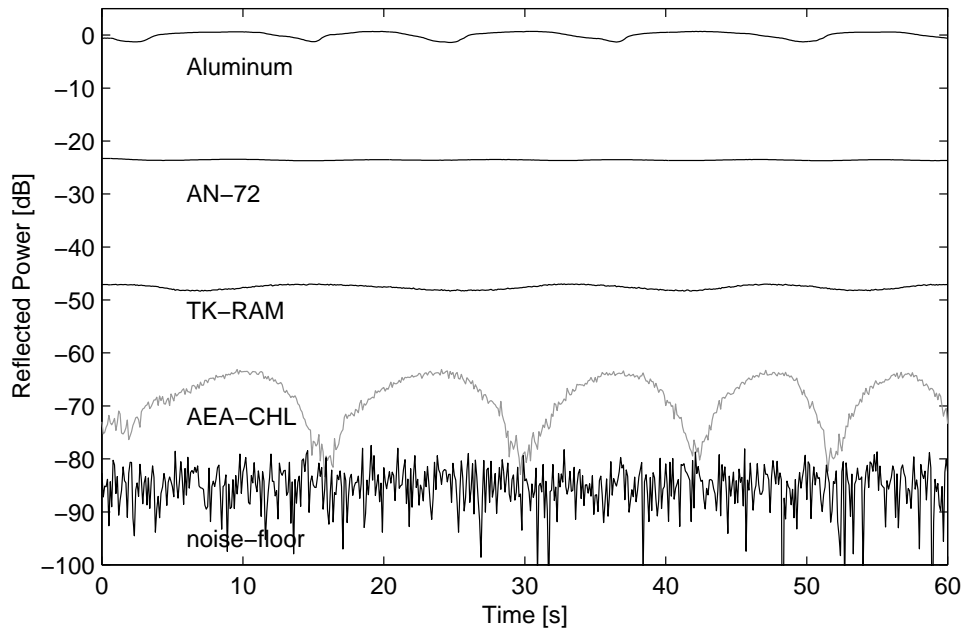


Figure 6: Reflection measurements of different microwave absorbers and the CHL at 406 GHz. The measurement of a flat aluminum plate was used to establish the 0 dB reference.

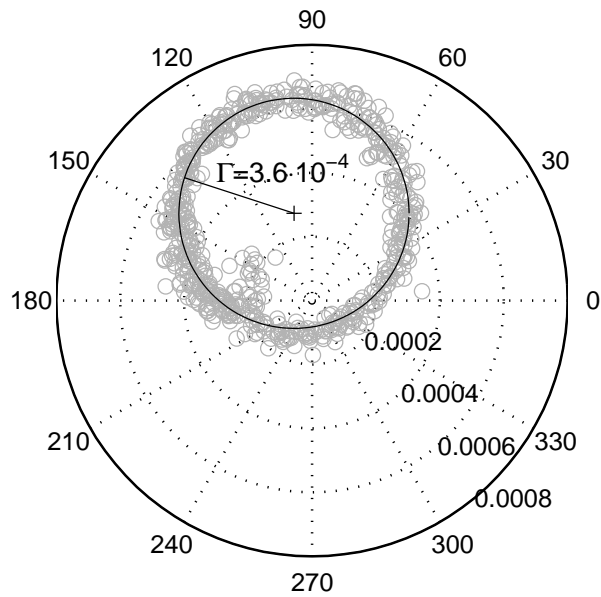


Figure 7: CHL measurement of figure 6 in polar coordinates on a linear scale. The solid circle represents the fit result of $\Gamma = 3.6 \cdot 10^{-4}$, which corresponds to a reflected power of about -69 dB.

Standing waves can also be generated by any other reflecting surfaces in the optical path, such as the windows in the cryostat and the aircraft, especially when they are placed close to perpendicular to the beam axis. For that reason parallel grooves were applied on both sides of the polyethylene aircraft window, which act as a $\lambda/4$ impedance matching layer. Measurements at 637 GHz with the reflectometer setup of figure 5 showed that the grooves have reduced the reflections below -24 dB compared to -17 dB of a window without impedance matching.

The same problems should arise at the surface of the liquid nitrogen in the cold load. But measurements have shown that this surface is disturbed by the natural boil-off of the nitrogen. At submillimeter wavelengths this leads to a fast random phase change of the reflected signal, which effectively cancels the baseline. This effect will be smaller at a longer wavelength, where the baseline from the cold load can be dominated by the surface of the nitrogen.

Another possible source of standing waves are reflections between the mixer and the local oscillator. They can appear in the calibrated spectra if the diplexer is not working correctly and if the impedance of the mixer is changed by the different power levels of the loads. Since this part of the quasi-optical path is not covered by the pathlength modulator, these baselines cannot be reduced with this device.

5 Baseline Error Simulations

This section will give an introduction in the retrieval of atmospheric parameters and an estimation of the baseline induced retrieval errors.

Following the formalism of Rodgers [15] the measured spectrum is represented by the measurement vector \mathbf{y} , which contains m elements for the discrete number of channels in the spectrometer. The atmospheric state is given by the vector \mathbf{x} , which contains the volume mixing ratio of the gas in a discrete number of n layers. Both are connected by the forward model F , which describes the radiative transfer equation through the atmosphere, and an additional measurement error ϵ :

$$\mathbf{y} = F(\mathbf{x}) + \epsilon \quad (6)$$

This can be linearised at a reference state \mathbf{x}_0 with $\mathbf{y}_0 = F(\mathbf{x}_0)$, using the weighting function $\mathbf{K} = \left. \frac{\partial F}{\partial \mathbf{x}} \right|_{\mathbf{x}_0}$:

$$\mathbf{y} = \mathbf{y}_0 + \mathbf{K}(\mathbf{x} - \mathbf{x}_0) + \epsilon \quad (7)$$

The inverse problem is the retrieval of the unknown atmospheric state $\hat{\mathbf{x}}$ from the measurement:

$$\hat{\mathbf{x}} = \mathbf{x}_0 + \mathbf{D}(\mathbf{y} - \mathbf{y}_0) \quad (8)$$

To calculate the contribution function \mathbf{D} it is necessary to introduce some form of additional information, because the the matrix \mathbf{K} is always close to being singular. A commonly used inversion technique for that purpose is the optimal estimation method [15] (OEM), which combines both the measurements and the a priori estimate \mathbf{x}_0 in a statistically optimal way:

$$\mathbf{D} = (\mathbf{K}^T \mathbf{S}_y^{-1} \mathbf{K} + \mathbf{S}_x^{-1})^{-1} \mathbf{K}^T \mathbf{S}_y^{-1} \quad (9)$$

\mathbf{S}_y is the covariance of the measurement errors. The uncertainty of the a priori profile \mathbf{x}_0 is described by the a priori covariance matrix \mathbf{S}_x . The retrieval errors due to the measurement errors can be calculated using:

$$\Delta \hat{\mathbf{x}} = \hat{\mathbf{x}} - \mathbf{x} = \mathbf{D}\epsilon \quad (10)$$

To estimate the influence of the baselines, we made a series of simulated CIO retrievals with varying baseline periods. The phase of each baseline was chosen to get a cosine function symmetric to the line centre, which covers the worst case for the retrieval. The baseline amplitude was assumed to be 0.1 K, and the covariance matrix \mathbf{S}_y was calculated for an uncorrelated radiometric noise with 0.35 K rms. Figure 8 displays the errors $\Delta \hat{\mathbf{x}}$ of the retrieved CIO profiles depending on the altitude and the baseline period. They show a characteristic pattern with maximum values of ± 0.3 ppb in the lower stratosphere. This can be compared to the CIO concentration under normal atmospheric conditions, which has a maximum of about 0.6 ppb at an altitude of 40 km and much smaller values at lower altitudes.

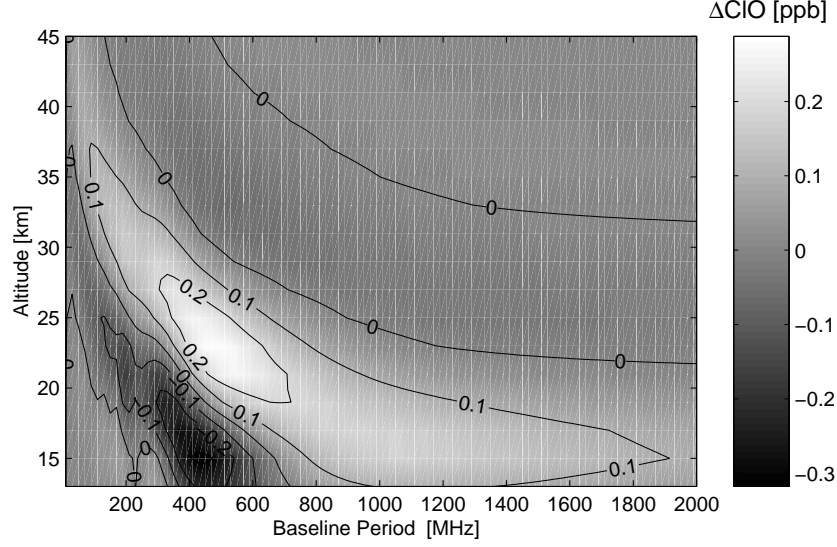


Figure 8: Effect of baselines with 0.1 K amplitude on the retrieval, depending on the baseline period.

6 Baseline Retrieval

The simulations in the last section demonstrate the need of a baseline correction within the retrieval. Nedoluha et al. [13] proposed to include the baseline errors in the error covariance matrix \mathbf{S}_y of the OEM. We followed the approach of Kuntz et al. [9], which allows a simultaneous retrieval of the atmospheric parameters together with a fit of the baseline. In this case the baseline is represented by:

$$\epsilon_{base} = a \sin(k\nu) + b \cos(k\nu) \quad (11)$$

The baseline period $2\pi/k$ must be known prior to the retrieval or can be determined from a Fourier transformation of the residuals after a first iteration step. The amplitudes a and b are treated as free parameters within the inversion process by replacing the state vector and the weighting function in equation 7 with:

$$\mathbf{x}' = \begin{bmatrix} \mathbf{x} \\ a \\ b \end{bmatrix} \quad \mathbf{K}' = \begin{bmatrix} K_{11} & \cdots & K_{1n} & \sin(k\nu_1) & \cos(k\nu_1) \\ \vdots & \ddots & \vdots & \vdots & \vdots \\ K_{m1} & \cdots & K_{mn} & \sin(k\nu_m) & \cos(k\nu_m) \end{bmatrix} \quad (12)$$

The fit of the parameters a and b is not an ill posed problem like the atmospheric retrieval and does not require any a priori constraints. Thus the inverse of the a priori covariance matrix in equation 9 can be rewritten as:

$$\mathbf{S}_x^{-1'} = \begin{bmatrix} \mathbf{S}_x^{-1} & 0 & 0 \\ 0 & 0 & 0 \\ 0 & 0 & 0 \end{bmatrix} \quad (13)$$

This method can be adapted in a similar way for the inversion of several baselines with different periods. It has proved to be very useful for the retrieval of atmospheric profiles from measurements disturbed by standing waves. Figure 9 shows a measurement of the CIO line with a 0.2 K baseline. The period of 216 MHz indicates a distance of $d = 0.7$ m, which corresponds to the distance between the mixer and the local oscillator. In this case the simultaneous baseline retrieval gives an significant improvement of the CIO results.

It should be pointed out that any kind of baseline correction can only be applied if it is possible to distinguish between the baseline and the spectral line features. This requires that the measured spectrum contains more than one period of the standing waves. Otherwise the sensitivity of the retrieval will be reduced in the lower altitudes.

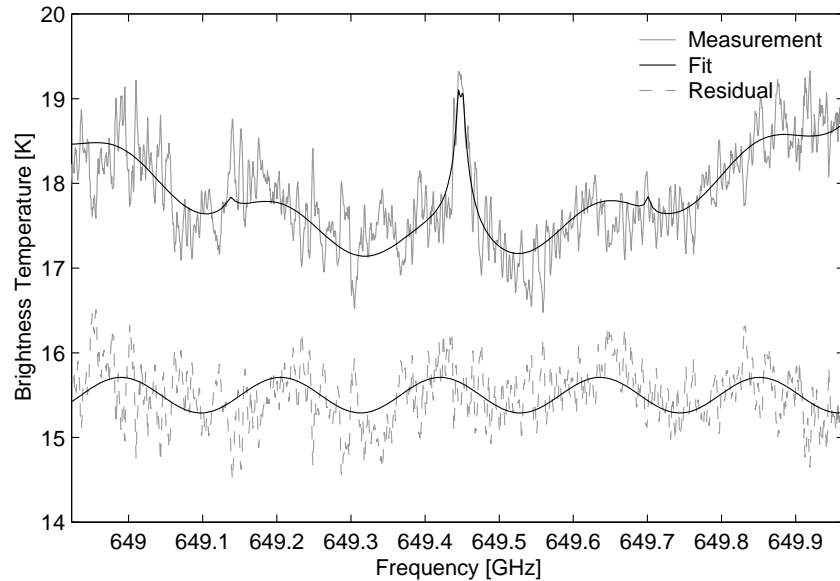


Figure 9: CIO measurement and residuals after a simultaneous retrieval of the atmospheric parameters and the baseline.

7 Conclusions

Baselines due to standing waves are a serious problem in millimeter and submillimeter wave radiometry. In this paper we gave an overview of these aspects at the example of an airborne 650 GHz receiver. A common technique for the baseline reduction is the use of a pathlength modulator. Both theory and measurements have shown that the performance of such a device is improved by using a linear instead of a sinusoidal variation of the pathlength. Further improvements could be achieved with calibration loads with a lower reflectivity. We have presented first vector measurements of a novel calibration load, which are showing very promising results. We also discussed the impact of the standing waves on the retrieval of atmospheric profiles and an inversion algorithm which allows a correction of the baseline errors.

Acknowledgements

This work was funded by the Swiss National Science Foundation under grant 2000-049426.96/1 and the European Space Agency. We wish to thank the Swiss Airforce for their support during the flight campaigns and Nigel Keen and Richard Wylde for valuable discussions concerning the load measurements.

References

- [1] Susanne Crewell. *Submillimeter-Radiometrie mit einem Flugzeuggetragenen Empfänger zur Messung atmosphärischer Spurenstoffe*. Reihe Umwelttechnik. Shaker, Aachen, 1993.
- [2] Emerson&Cuming Microwave Products. Massachusetts, U.S.A.
- [3] R.H. Giles, A.J. Gatesman, J.F. Gerald, S. Fisk, and J. Waldman. Tailoring artificial dielectric materials at terahertz frequencies. In *The Fourth International Symposium on Space Terahertz Technology*, Los Angeles, April 1993.
- [4] P. F. Goldsmith and N. Z. Scoville. Reduction of baseline ripple in millimeter radio spectra by quasi-optical phase modulation. *Astron. Astrophys.*, 82, April 1980.

- [5] P. Goy, M. Gross, and S. Caroopen. Millimeter and submillimeter vector measurements with a network analyzer up to 1000 GHz. Basic principles and applications. Technical report, AB Millimetre, Paris, France, May 1998.
- [6] J. J. Gustincic. A quasi-optical receiver design. In *IEEE Conference Proceedings on MTT*, pages 99–100, San Diego, 1977.
- [7] Nigel Keen, Rob Spurrett, and Richard Wylde. An absolute blackbody source for radiometer calibration at submillimeter wavelength. In *ESA Workshop on Millimetre Wave Technology and Applications*, pages 4.2.1–4.2.10, Noordwijk, December 1995. European Space Agency.
- [8] Nigel J. Keen. Broad-band microwave measurements of receiver noise temperature and antenna temperature. *Proc. German URSI Conference, Kleinheubach*, pages 485–495, 1973.
- [9] M. Kuntz, G. Hochschild, and R. Krupa. Retrieval of ozone mixing ratio profiles from ground-based millimeter wave measurements disturbed by standing waves. *J. Geophys. Res.*, 102(D18):21,965–21,975, September 1997.
- [10] Jens Langer. *Charakterisierung eines Radiometers für atmosphärenphysikalische Messungen*. Diploma thesis, University of Bremen, 1995.
- [11] Axel Murk. *Aufbau und Einsatz eines flugzeuggetragenen Submillimeter-Empfärs für die Bestimmung von stratosphärischem ClO, HCl und O₃*. PhD thesis, University of Bern, Switzerland, 1999.
- [12] Axel Murk, Niklaus Kämpfer, and Nigel Keen. Baseline measurements with a 650 GHz radiometer. In J. Mallat, A. Räisänen, and J. Tuovinen, editors, *Proceedings of 2nd ESA Workshop on Millimetre Wave Technology and Applications: Antennas, Circuits and Systems*, pages 121–126, Espoo, Finland, May 1998. MilliLab.
- [13] Gerald E. Nedoluha, Richard M. Bevilacqua, R. Michael Gomez, D. L. Thacker, William B. Waltman, and Thomas A. Pauls. Ground-based measurements of water vapor in the middle atmosphere. *J. Geophys. Res.*, 100(D2):2927–2939, February 1995.
- [14] A. Parrish, R. L. de Zafra, P. M. Solomon, and J. W. Barrett. A ground-based technique for millimeter wave spectroscopic observations of stratospheric trace constituents. *Radio Sci.*, 23(2):106–118, March–April 1988.
- [15] C. D. Rodgers. Retrieval of atmospheric temperature and composition from remote measurements of thermal radiation. *Rev. Geophys. Space Phys.*, 14(4):609–624, November 1976.
- [16] Kristen Rohlfis. *Tools of Radio Astronomy*. Astronomy and astrophysics Library. Springer Verlag, Berlin, 1986.
- [17] Thomas Keating Ltd. Billingshurst, U.K.